A Terrestrial Validation of ICESat Elevation Measurements and Implications for Global Reanalyses

Adrian A. Borsa, Helen Amanda Fricker, and Kelly M. Brunt

***Abstract*— The primary goal of NASA's Ice, Cloud, and land Elevation Satellite (ICESat) mission was to detect centimeter-level changes in global ice sheet elevations at the spatial scale of individual ice streams. Confidence in detecting these small signals requires careful validation over time to characterize the uncertainty and stability of measured elevations. A common validation approach compares altimeter elevations to an independently characterized and stable reference surface. Using a digital elevation model (DEM) from geodetic surveys of one such surface, the salar de Uyuni in Bolivia, we show that ICESat elevations at this location have a 0.0-cm bias relative to the WGS84 ellipsoid, 4.0-cm (1-sigma) uncertainty overall, and 1.8-cm uncertainty under ideal conditions over short (50 km) profiles. We observe no elevation bias between ascending and descending orbits, but we do find that elevations measured immediately after transitions from low to high surface albedo may be negatively biased. Previous studies have reported intercampaign biases (ICBs) between various ICESat observation campaigns, but we find no statistically significant ICBs or ICB trends in our data. We do find a previously unreported 3.1-cm bias between ICESat's Laser 2 and Laser 3, and we find even larger interlaser biases in reanalyzed data from other studies. For an altimeter with an exact repeat orbit like ICESat, we also demonstrate that validation results with respect to averaged elevation profiles along a single ground track are comparable to results obtained using reference elevations from an *in situ* survey.**

***Index Terms*— Ice sheets, laser ranging, lidar, remote sensing, satellite laser altimetry, system validation.**

I. Introduction

SATELLITE altimeters estimate Earth surface elevations by precisely measuring the roundtrip travel time of electromagnetic pulses from the spacecraft to the surface and back. In Earth's polar regions, the ability of satellite altimeters to monitor changing ice surface elevations over long periods makes them one of the primary means of assessing contemporary changes in the volume of the ice sheets [13], [14], [18], [34], [42], [43], [52], [55]. Altimeter measurements must meet high standards for accuracy and precision, since even small height changes over the large expanse of the Greenland and Antarctic ice sheets would imply significant changes in global sea level. To meet these standards, altimeters undergo extensive prelaunch and postlaunch efforts to identify (validate) and correct (calibrate) measurement error from various sources [1], [2], [12], [27], [44], [46], [47], [54]. This process is commonly referred to as calibration and validation, or "Cal/Val." A widely used technique for satellite altimetry Cal/Val is postlaunch (or on-orbit) comparison of altimeter elevations with independently surveyed reference elevations within the flat interiors of the ice sheets [16], [23], [24], [33], [45], [58] or in arid environments with little vegetation or surface change [10], [19], [28]. These analyses can provide an assessment of altimeter performance over the span of an entire mission and can be used to cross-calibrate different altimeters to unify observations of surface elevation change across multiple instruments and missions [11].

This paper specifically focuses on the validation of elevations from NASA's Ice, Cloud, and land Elevation Satellite (ICESat) laser altimeter. ICESat (launched on January 12, 2003 and decommissioned on August 14, 2010) was an altimeter mission whose primary objective was to assess elevation changes on the polar ice sheets [41], [51], [56]. ICESat used a single-beam waveform recording laser altimeter [the Geoscience Laser Altimeter System (GLAS)] to sample Earth's surface. Each laser pulse illuminated a 50–100-m-diameter surface "footprint," and consecutive footprints were spaced every 170 m along the satellite ground track. Reflected laser light from each footprint was recorded by the ICESat detector and digitized into a "return waveform" of energy versus time, which was processed to estimate the average footprint elevation. ICESat's altimeter did not acquire data continuously, but was operated in a series of approximately 1 month "campaigns" separated by 2–6 month periods when the laser was switched off (Table I, [51]).

Various studies have reported on the validation of ICESat elevations using independently surveyed elevation profiles on ice sheets as a reference. Hofton *et al.* [23] compared ICESat to a 350-km airborne laser altimeter traverse along 86°S, finding relative biases of −3.6 to +14.7 cm and standard deviations of 0.8–5.5 cm, depending on the campaign.

Manuscript received July 19, 2018; revised January 27, 2019; accepted March 31, 2019. Date of publication May 24, 2019; date of current version August 27, 2019. This work was supported by the NASA's Research Opportunities in Space and Earth Sciences Program under Grant NNX12AG67G and Grant NNX15AC80G. *(Corresponding author: Adrian A. Borsa.)*

A. A. Borsa and H. A. Fricker are with the Scripps Institution of Oceanography, University of California at San Diego, San Diego, CA 92093 USA (e-mail: aborsa@ucsd.edu).

K. M. Brunt is with the Earth System Science Interdisciplinary Center, University of Maryland at College Park, College Park, MD 20740 USA, and also with the NASA Goddard Space Flight Center, Greenbelt, MD 20771 USA.

Color versions of one or more of the figures in this article are available online at http://ieeexplore.ieee.org.

Digital Object Identifier 10.1109/TGRS.2019.2909739

TABLE I
ICESAT CAMPAIGN METADATA

	Campaign	Laser #	Start date	End date	Reference Orbit	Transmit Energy (mJ)	# Days
calibration	L1a	Laser 1	2/20/03	3/21/03	8-day		29
	L1b	Laser 1	3/21/03	3/29/03	8-day		9
	L2a	Laser 2	9/25/03	10/4/03	8-day		9
operational phase	L2a	Laser 2	10/4/03	10/13/03	91-day		9
	L2a (post dT)	Laser 2	10/13/03	11/19/03	91-day	66.1	37
	L2b	Laser 2	2/17/04	3/21/04	91-day	40.6	34
	L2c	Laser 2	5/18/04	6/21/04	91-day	9.6	35
	L3a	Laser 3	10/3/04	11/8/04	91-day	61.6	37
	L3b	Laser 3	2/17/05	3/24/05	91-day	56.7	36
	L3c	Laser 3	5/20/05	6/23/05	91-day	44.8	35
	L3d	Laser 3	10/21/05	11/24/05	91-day	39.0	35
	L3e	Laser 3	2/22/06	3/28/06	91-day	33.1	34
	L3f	Laser 3	5/24/06	6/26/06	91-day	31.6	33
	L3g	Laser 3	10/25/06	11/27/06	91-day	26.5	34
	L3h	Laser 3	3/12/07	4/14/07	91-day	22.1	34
	L3i	Laser 3	10/2/07	11/5/07	91-day	20.7	35
	L3j	Laser 3	2/17/08	3/21/08	91-day	17.4	34
	L3k	Laser 3	10/4/08	10/19/08	91-day	13.5	16
	L2d	Laser 2	11/25/08	12/17/08	91-day	6.0	23
	L2e	Laser 2	3/9/09	4/11/09	91-day	2.8	34
	L2f	Laser 2	9/30/09	10/11/09	91-day		12

L2a (post dT) is the period after the insteument temperature spike (dT) on 10/13/2003. Data Source: NSIDC (https://nsidc.org/data/icesat/laser_op_periods.html)

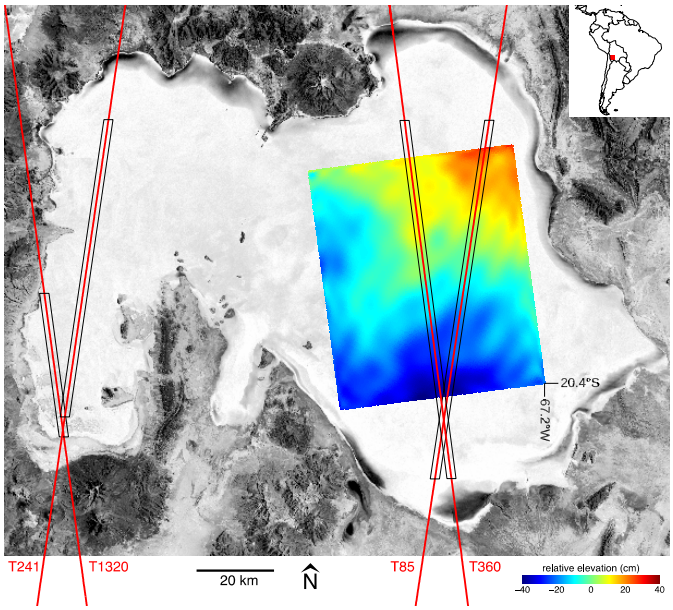

Fig. 1. Landsat image of the salar de Uyuni, showing ICESat Tracks 85, 241, 360, and 1320 (red) and the GPS-derived DEM from 2009 (color-coded with respect to mean elevation). The portion of each track plotted in Fig. 2 is boxed in black. Total relief on the GPS DEM is less than 1 m over 50 km.

Siegfried *et al.* [45] compared part of an 11-km kinematic global positioning system (GPS) traverse near Summit Station, Greenland with ICESat elevations from four campaigns. They reported relative biases of −11.1 to +12.1 cm between the two data sets, with standard deviations of 2.7–7.1 cm. Kohler *et al.* [24] compared ICESat elevations with contemporaneous kinematic GPS data collected along a 10 000-km traverse of the East Antarctic Ice Sheet for five campaigns and reported relative biases of −14.2 to +24.5 cm and standard deviations of 10.3−18.7 cm. Traverse-based validations such as these are valuable, but errors in the kinematic GPS used to position the survey platform can result in time-correlated noise with amplitudes up to 10 cm over several hours [7], suggesting that a significant portion of the reported error is likely to be in the reference data set. These studies also assumed that the ice sheet surface itself did not undergo any height change over the ICESat mission, which is possible but not verifiable using ICESat alone.

Here, we present a new comprehensive validation of ICESat elevations using an alternative technique that relies on a digital elevation model (DEM) of a densely surveyed terrestrial reference surface, the salar de Uyuni in the Bolivian Altiplano (20.2°S, 67.6°W). The 9600 km^2 salar is the largest dry lake on Earth (Fig. 1) and is well suited for laser altimeter Cal/Val due to its size, lack of topography, uniformly high albedo [37], and minimal surface deformation. The salar is actively leveled by shallow flooding during the January–March wet season, producing a smooth surface that can be surveyed by vehicle using kinematic GPS [9].

The salar de Uyuni provided the first terrestrial validation of ICESat elevations over a decade ago, with confirmation of forward scattering effects, increased noise with reduced laser energy, and range delays due to detector saturation [19]. We expand the previous analysis to encompass the full-mission data set processed to a single consistent standard, and to incorporate the results of a repeat survey of the salar de Uyuni in 2009, near the end of the ICESat mission. In addition to providing definitive estimates of ICESat elevation accuracy and precision, we investigated the premise that there are systematic global elevation biases between individual ICESat campaigns [also known as intercampaign biases (ICBs)] that are large enough to be observable in the ICESat data set [10], [23], [49]. Although our analysis did not find statistically significant ICBs or ICB trends at the salar de Uyuni, it did reveal a significant bias between ICESat's lasers that has not been reported elsewhere.

II. DATA SETS

A. ICESat Laser Altimetry

ICESat carried three lasers. Although all were manufactured to the same specifications [3], there was variability in the shape of the laser beam ([2], [59]), with Laser 1 and Laser 2 exhibiting an elongated elliptical footprint ∼100 m along its semimajor axis, and Laser 3 a roughly circular footprint ∼50 m in diameter.

Laser 1 operated while ICESat was in its initial 8-day exact repeat calibration orbit (January 20, 2003–October 4, 2003) and failed after 36 days. Laser 2 operated for 9 days in the 8-day orbit and thereafter in ICESat's primary 91-day exact repeat orbit. Laser 3 operated entirely in the 91-day orbit. To extend the life of Lasers 2 and 3, and to ensure that data were acquired over a longer time span for monitoring the ice sheets, ICESat was operated quasi-continuously in 18 discrete ∼33-day campaigns spaced 2–6 months apart and timed to occur in one of three windows: February/March (Antarctic spring), May/June (Antarctic winter), and October/November (Antarctic autumn) (Table I, [51], [60]). Campaigns are identified by the number of the operational laser followed by a letter designating each consecutive campaign for that laser (e.g., L2a is the first campaign for Laser 2).

Since most ice-sheet change studies omit data from Laser 1, this paper focuses on Lasers 2 and 3 only, commencing with data from campaign L2a after the temperature spike on October 13, 2003 [61].

ICESat's orbit was maintained close to a reference orbit throughout the mission, which ensured that laser footprints fell within several kilometers of fixed and repeating nadir ground tracks. In the polar regions and at selected mid-latitude targets of opportunity (TOOs), precision pointing of the spacecraft was used to steer the laser footprints to the reference ground tracks or to predetermined off-nadir locations. Each of the sampled ground tracks was overflown approximately once per campaign, and we refer to each repeat-track overflight as a "repeat." ICESat had two sets of ground tracks, one for the 8-day orbit and another one for the 91-day orbit. All tracks discussed in this paper are 91-day tracks.

Two ICESat tracks crossed the eastern lobe of the salar de Uyuni: descending (north-to-south) Track 85 and ascending (south-to-north) Track 360 (Fig. 1). Since the eastern salar was a TOO for mission Cal/Val, ICESat was programmed to precisely point to these tracks to ensure that the same topography was sampled during each repeat, similar to the pointing strategy implemented in polar regions. As a result, footprints from all repeats on these two tracks fell within a narrow 300-m-wide swath. Qualitatively, elevations along these tracks are broadly consistent over the mission [Fig. 2 (top)], with differences between campaigns primarily due to variability in: 1) orbit and pointing determination; 2) laser propagation through the atmosphere; and 3) other instrument and/or environmental effects not related to surface motion.

Two additional ICESat tracks crossed the salar: descending Track 241 and ascending Track 1320 (Fig. 1). These two tracks sampled the western lobe of the salar, whose topography exhibits larger-amplitude surface undulations than occur in the eastern lobe [6]. ICESat was not programmed to point at these tracks, which resulted in wider separation between repeat tracks: up to 2 km for Track 1320 and 4 km for Track 241. Elevations along these tracks [Fig. 2 (bottom)] are less consistent between various repeats than are elevations on Tracks 85 and 360.

We used ICESat elevations (d_elev) from the GLA06 (Global Elevation) data product available from the National Snow and Ice Data Center (NSIDC; http://nsidc.org/data/icesat/). These elevations were geolocated with respect to the ITRF2000 (campaigns L2a to L3g) and ITRF2005 (campaigns L3h to L2f) reference frames and vertically referenced to the TOPEX/Poseidon ellipsoid [48]. The 0.4×10^{-9} difference of scale between the two ITRF frames [4] causes a +2.5-mm offset in ICESat elevations on the salar de Uyuni starting in L3h, which we did not remove. We did make two other adjustments to ICESat elevations to align them to the GPS-derived Uyuni DEMs: 1) we transformed ICESat elevations to reference the WGS84 ellipsoid, which lowered all elevations on the salar de Uyuni by ~70.2 cm and 2) we transformed ICESat elevations from the mean-tide system in which they are provided to the tide-free system used by GPS, using the methodology from [30]. At the latitude of the salar de Uyuni, this tide correction lowers ICESat elevations by an additional 3.9 cm.

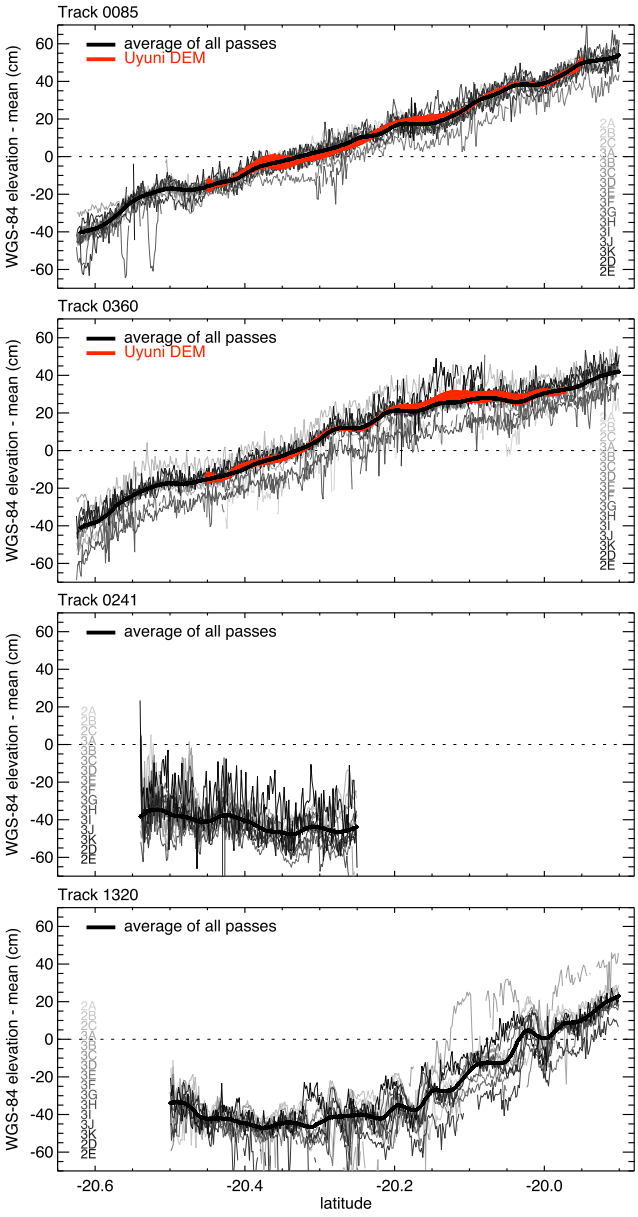

Fig. 2. Elevation profiles for all ICESat repeat along on Tracks 85 and 360 (left) and Tracks 241 and 1320 (right) over the salar de Uyuni (see location plot in Fig. 1). Profiles are shaded from light to dark gray to correspond to the time progression of the campaigns listed chronologically at the edge of each plot. The corresponding reference profiles from the GPS DEM (in red on Tracks 85 and 360) span the DEM elevations from 2002 to 2009. The averaged elevation profiles (thick black line in each plot) were estimated using data from all repeats on each track.

Some ICESat elevations were impacted by detector saturation, which occurred when surface-reflected received laser energy exceeded instrument design thresholds [46]. This occurred even though ICESat was pointed slightly off-nadir to minimize the chance of high-energy specular surface reflections. Detector saturation caused an increase in reported range and a corresponding decrease in elevation, which had to be corrected to produce unbiased ICESat elevations. For all data in this paper, we corrected for detector saturation following the

TABLE II
ICESAT DATA RELEASES

Release	YXX	GSAS	Date	Notes
12	112	v3.6	8/27/03	
13	113	v3.7	12/5/03	
14	314	v3.8	2/10/04	
17	317	v3.9	5/5/04	major release for atmospheric products
18	318	v4.0	8/16/04	
19	319	v4.1	12/10/04	
21	421	v4.2	3/10/05	
22	322	v4.3	5/12/05	
24	424	v5.0	10/11/05	saturation correction for gain 13
26	426	v5.2	1/31/06	major release: saturation correction for all gains
28	428	v5.3	8/31/06	major release: improved saturation correction
29	529	v5.4	6/25/08	major release: improved elevation/waveform processing
31	531	v5.6	8/28/09	major release: improvements for low transmit power
33	633	v6.0	3/10/11	major release: saturation correction, pointing
34	634	v6.1	1/31/14	major release: G-C range correction

I-SIPS Product Release numbers (Release) were incremented with each version of GLAS Science Algorithm Software (GSAS). We use the 2-digit I-SIPS numbering convention in this paper, but list the highest 3-digit Elevation Product Release number (YXX) for reference. Shaded releases are those whose results we compare in Fig. 6. Data source: NSIDC (https://nsidc.org/data/icesat/data_releases.html; https://nsidc.org/data/icesat/yxx_release_numbers.html)

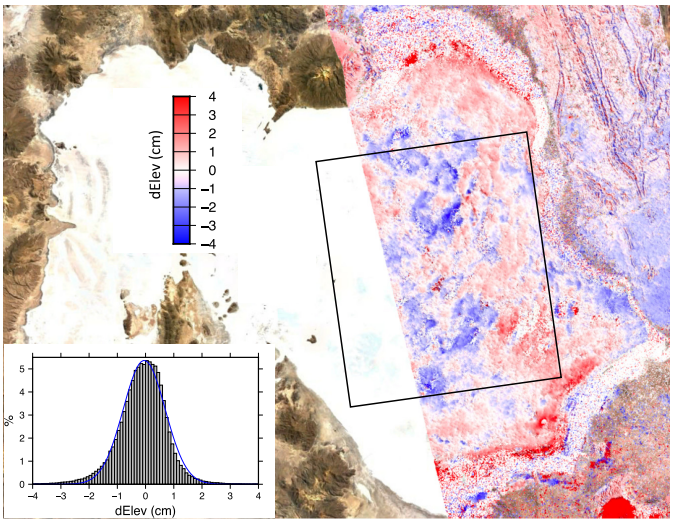

Fig. 3. ALOS InSAR interferogram showing the 1-year elevation change on the salar de Uyuni between August 24, 2009 and August 27, 2010, coinciding with the end of the ICESat mission. The portion of the scene lying within the GPS DEM (black outline) exhibited overall elevation change of 0.0 ± 0.7 cm (1σ), distributed as shown in the histogram at lower left.

recommended methodology in [46], adding the GLA06 parameter i_satElevCor to the reported elevation for each footprint.

ICESat data processing evolved throughout the mission to take advantage of new algorithms and improved calibrations. The existing data sets were routinely reprocessed, with the results made publicly available in a series of data releases (Table II). Release 34 was the final and definitive release, and the names of all parameters referenced in this paper follow Release 34 conventions. Although Releases 33 and 34 are the only ones currently available at NSDIC, we present results for selected prior releases to show how ICESat geolocation accuracy changed over time. The "G minus C" (or G−C) elevation correction [10] was included in the standard processing of Release 34 data only, and we did not retroactively apply the G−C correction to earlier releases.

B. GPS Reference DEMs of the Salar de Uyuni, Bolivia

We conducted GPS surveys of a 54-km × 45-km region in the eastern lobe of the salar de Uyuni (Fig. 1) in September of both 2002 and 2009. We drove the same route in both surveys, dividing the survey region into eight equal-area rectangular grids and surveying each grid independently [9]. Each survey had a static and a kinematic component, with four fixed GPS base stations providing static control for postprocessing the kinematic GPS trajectories. We operated one fixed GPS base station at the center of the survey region continuously for the survey duration. The other three fixed stations were used in a rolling deployment, operating for 24 h along the perimeters of the grids being surveyed kinematically that day. The kinematic survey was carried out using vehicle-mounted GPS, sampling at 1/3 Hz in 2002 and 1 Hz in 2009. To correct for height changes due to fuel consumption, we measured the vehicle antenna height before and after each survey and linearly interpolated the change to each GPS epoch based on distance driven. Borsa *et al.* [8] provide details of the survey methodology and data postprocessing.

GPS equipment slightly varied between surveys, but all included dual-frequency receivers (Ashtech Z-12 in 2002, Topcon GB-1000 in 2009) and geodetic-quality antennae (Ashtech choke ring in 2002, Topcon PG-A1 in 2009). We processed the GPS in the IGS05 reference frame (which is aligned to ITRF2005), with base station positions estimated using the Scripps Coordinate Update Tool (SCOUT) from the Scripps Orbit and Permanent Array Center (sopac.ucsd.edu), and kinematic trajectories calculated using track, the kinematic module of Massachusetts Institute of Technology's GAMIT processing package.

Elevation profiles derived from kinematic GPS are impacted by decimeter-level correlated noise due to unmodeled multipath and troposphere effects [7]. Using the methodology in [7], we corrected the elevation profiles using constraints provided by crossover points in the survey grid and by the known elevations of the fixed GPS sites. Using the corrected elevation profiles, we generated WGS84-referenced DEMs of the survey region, which fit the underlying GPS elevations at the subcentimeter level [8].

Topographic relief over the 2400 km^2 Uyuni DEMs is only 80 cm, dominated by an elevation ramp from the southwest to northeast and by decimeter-amplitude topography correlated over distances of several kilometers and greater (Fig. 1). From elevation comparisons between the main 2002 DEM and two additional semioverlapping grids which we surveyed only in that year, we estimated DEM error to be 1.5-cm root mean square (rms).

C. Generation of Reference Elevations and Calculation of Elevation Differences

We used two approaches for generating reference elevations for our analysis: 1) the DEM method and 2) the repeat-track method.

1) DEM Method: This method used the GPS-derived DEMs of the salar de Uyuni as an elevation reference, with bilinear interpolation between DEM nodes providing a reference elevation for each ICESat footprint on Tracks 85 and 360. Using the

two DEMs, we generated separate reference elevations for 2002 and 2009, then linearly interpolated in time to obtain an intermediate reference elevation corresponding to the date of each repeat [10] (Fig. 2, red band of elevations). This approach assumed that any topographic change between 2002 and 2009 occurred uniformly in time, which was the simplest assumption we could make and is consistent with our discussion of surface variability in Section III-E. We created a data set of elevation differences by subtracting reference elevations from ICESat elevations for all coincident laser footprints with detectable received energy. This yielded elevation residuals for 8381 footprints on 30 ICESat repeats, split equally between Tracks 85 and 360.

2) Repeat-Track Method: This method used the average elevation of all footprints on a single track as an elevation reference (Fig. 2, thick black lines), bypassing the need for a reference DEM and extending our analysis beyond our DEM boundaries and to additional ICESat tracks.

For each of the four ICESat tracks over the salar de Uyuni, we generated reference elevation profiles sampled every 100 m, with values taken from a Hamming-weighted average of all footprint elevations located within $\pm$ 2.5 km along track. Prior to averaging, we removed outliers whose elevations lay more than two times the interquartile range (IQR) from the median elevation within each window. The specific procedure used for creating the reference profiles was less important than ensuring that the profiles were not biased by outliers and were as smooth as the GPS-derived DEMs, which represent almost all the variability in the underlying surface [7]. We also note that this technique was viable because of the low across-track slopes on the salar (median value 7×10^{-6}) and small across-track distances between ICESat repeats (300 m for Tracks 85 and 360; 2–4 km for Tracks 241 and 1320), which minimized the error from having repeats that did not exactly sample the same surface profiles. We obtained elevation differences for 20 065 footprints from 59 ICESat repeats along Tracks 85, 241, 360, and 1320. Although this method did not provide an assessment of ICESat's absolute elevation accuracy, it did allow us to use altimetry data beyond the Uyuni DEM, more than doubling the number of elevation residuals in our analysis.

D. InSAR Estimates of salar de Uyuni Surface Deformation

For an independent estimate of surface deformation on the salar de Uyuni, we obtained coincident Advanced Land Observation System (ALOS) PALSAR L-band synthetic aperture radar (SAR) scenes from Track 97 on October 4, 2007, August 24, 2009, August 27, 2010, and January 2, 2011. We used fine mode level 1.5 multilook amplitude/phase data and generated interferograms between these scenes using the open-source GMT5SAR software [38], obtaining estimates of surface deformation at 100-m resolution over 80-km-wide data swaths (Fig. 3). Although InSAR (Interferometric SAR) deformation is subject to errors from unmodeled atmospheric propagation delay, tropospheric error is minimized at the high elevation of the salar de Uyuni, and we chose pairs that showed no evidence of ionospheric error (e.g., light/dark banding) in the SAR amplitude image.

III. Results

Our estimates of ICESat elevation accuracy and precision were derived from the sample statistics of the elevation residuals, i.e., the differences between ICESat elevations and the reference elevations. For the purpose of this analysis, we define accuracy to be the median value of a set of residuals (the bias of the residuals) and precision to be the robust standard deviation of those residuals about their mean value (the scatter of the residuals), where the robust standard deviation is 0.74 of IQR. We report accuracy and precision as median $\pm$ robust standard deviation. Although a portion of the residual is due to uncertainty in the reference elevations themselves (1.5-cm rms in the case of the DEM method), for the sake of simplicity, we will refer to the combined accuracy/precision statistics as the ICESat elevation error.

A few points of clarification about our methodology and reporting are as follows.

1) Unless otherwise noted, we used the final Release 34 ICESat data set throughout the analysis.
2) On-orbit calibration tests for the ICESat saturation correction (henceforth, "saturation tests") were carried out on Track 360 during campaigns L3e, L3f, L3g, L3h, and L3j [46]. For these tests, the instrument gain (which adjusted the power of received signal to match the dynamic range of the ICESat signal detector) was fixed to anomalously high values to induce detector saturation, and the DEM bias for these repeats was used to tune the saturation correction. This combination of high gain and relatively high received energy is unlikely to occur elsewhere in the ICESat data set, since during normal operation the GLAS instrument automatically adjusted gain downward when high return energies were detected. We report elevation errors with and without these repeats, noting that statistics without these repeats are likely to be more representative of the statistics of the ICESat data set as a whole.
3) Our results omit footprints for which the elevation error due to detector saturation exceeded the limits of the saturation correction (0.6–1.8 m depending on gain), resulting in undefined values for GLA06 parameter i_satElevCor. Most of the affected footprints occurred in campaign L3b, when a thin layer of water on the salar surface resulted in specular reflections whose unusually high return energies saturated the detectors beyond the levels reached in engineering tests [46].

A. Assessment of ICESat Elevation Quality Using the DEM Method

1) ICESat Elevation Accuracy and Precision: For the 8381 ICESat footprints coinciding with the Uyuni DEM, the elevation error with respect to the DEM was -0.4 ± 4.6 cm [Table III, blue and red points in Fig. 4(a)]. We note that not applying the saturation correction yielded an error of -3.7 ± 8.9 cm, which was significantly worse than that for saturation-corrected elevations. For the subset of 6914 footprints that excluded the saturation test data [blue points in Fig. 4(a)], the error was reduced to 0.0 ± 4.0 cm. The distribution of residuals was nominally Gaussian [Fig. 4(a), right]

TABLE III

ICESAT ELEVATION ERROR: SUMMARY STATISTICS

	Gain	N	*E* (fJ)	% Sat	DEM Error (cm)	Repeat-track Error (cm)	Difference (cm)
All data	17	8381	7.9	46	-0.4 ± 4.6	-0.2 ± 4.3	-0.2 / 0.3
omitting saturation test data	15	6914	8.1	41	0.0 ± 4.0	0.1 ± 3.8	0.0 / 0.2
Laser 2	29	2131	3.6	15	1.7 ± 4.6	1.6 ± 4.5	0.1 / 0.1
Laser 3	16	6250	9.4	57	-1.1 ± 4.6	-0.7 ± 4.4	-0.4 / 0.2
omitting saturation test data	13	4783	15.9	53	-0.7 ± 3.8	-0.4 ± 3.6	-0.3 / 0.2
Track 85	15	4219	8.9	43	0.0 ± 4.5	0.0 ± 4.2	0.0 / 0.3
Track 360	26	4162	7.1	49	-0.7 ± 4.9	-0.3 ± 4.7	-0.4 / 0.2
omitting saturation test data	16	2695	7.3	38	0.1 ± 3.5	0.3 ± 3.5	-0.2 / 0.0
Gain ≤ 20 (Low Gain)	13	4861	17.2	58	0.0 ± 3.4	-0.1 ± 3.2	0.0 / 0.2
no saturation correction	16	2052	7.2	0	-0.5 ± 3.3	-0.5 ± 3.3	-0.1 / 0.0
saturation corrected	13	2809	20.6	100	0.3 ± 3.3	0.2 ± 3.1	0.1 / 0.3
20 < Gain ≤ 50	26	1801	4.4	14	0.2 ± 4.1	0.7 ± 4.0	-0.5 / 0.2
no saturation correction	28	1542	4.3	0	0.3 ± 4.2	0.8 ± 4.1	-0.5 / 0.1
saturation corrected	26	259	21.7	100	-0.5 ± 3.5	0.0 ± 2.9	-0.5 / 0.5
Gain > 50 (High Gain)	80	1719	1.9	46	-6.2 ± 11.5	-5.3 ± 12.1	-0.8 / -0.6
no saturation correction	68	924	1.4	0	2.3 ± 10.3	3.7 ± 9.8	-1.4 / 0.5
saturation corrected	128	795	8.5	100	-11.2 ± 4.7	-10.7 ± 4.4	-0.5 / 0.3

Column 2 lists the median gain (Gain), number of footprints (*N*), median return energy (*E*), and percentage of pulses that have a non-zero saturation correction (%Sat). Columns 3 and 4 show the median ± robust standard deviation for the residual difference between ICESat elevations and two references: the salar de Uyuni DEM (the DEM Method) and the averaged track elevation profile (the Repeat-track Method). Column 5 is the difference between the statistics derived from the DEM and Repeat-track methods. Results highlighted in grey appear in the text.

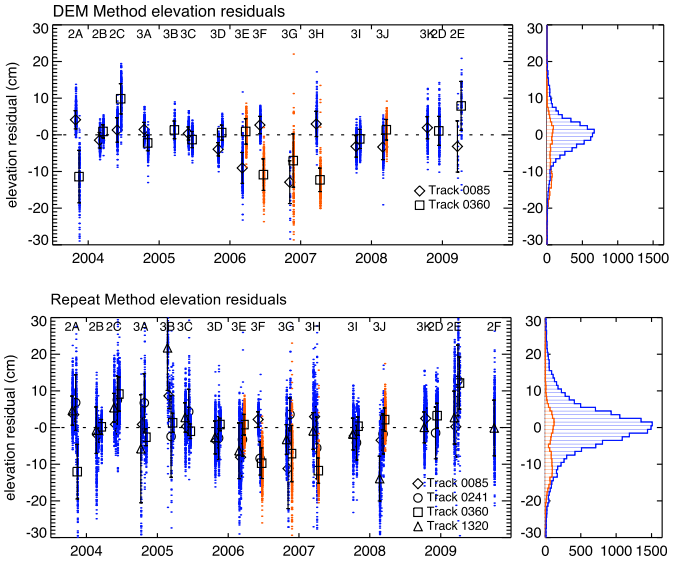

Fig. 4. (Top) Elevation residuals for all repeats of ICESat Tracks 85 and 360 with respect to the salar de Uyuni DEM (DEM method). Each vertical line of more than 300 points shows the residuals for all ICESat footprints on a single repeat. The diamonds and squares show the residual median for each repeat, and the error bars show the standard deviations. Campaigns in red are associated with the saturation calibration tests. (Right) Histogram of elevation residuals used in the saturation tests (red) and those that were not (blue). (Bottom) Same as (a) but showing elevation residuals relative to the average of all repeats (repeat-track method). We include residuals from Tracks 241 and 1320 in the western salar de Uyuni (Fig. 1).

but did not pass the Kolmogorov–Smirnov (K–S) test for a Gaussian distribution, suggesting that there were one or more sources of ICESat elevation error which were not white noise processes.

We assumed that a component of the elevation error was due to geolocation biases (e.g., from imprecise orbit determination

TABLE IV

ICESAT ELEVATION ERROR: REPEAT STATISTICS

	Campaign	Gain	N	angle	*E*	% Sat	DEM Error (cm)	Repeat-track Error (cm)	Difference (cm)
Track 85	L2a	13	321	0.29	22.3	100	4.1 ± 2.5	3.9 ± 1.8	0.2 / 0.7
	L2b	14	321	0.32	9.4	1	-1.5 ± 2.1	-2.0 ± 1.8	0.5 / 0.3
	L2c	30	320	0.33	3.6	0	1.3 ± 3.3	0.9 ± 2.6	0.4 / 0.7
	L3a	13	321	0.32	17.9	100	1.5 ± 1.9	1.1 ± 1.6	0.3 / 0.4
	L3b	13	320	0.32	84.1	100	(no valid data)	(no valid data)	
	L3c	13	321	0.32	16.4	100	0.4 ± 1.8	0.1 ± 1.6	0.2 / 0.1
	L3d	13	321	0.31	16.1	100	-3.9 ± 1.8	-3.9 ± 1.7	-0.1 / 0.1
	L3e	17	321	0.37	7.9	46	-9.0 ± 4.2	-9.0 ± 3.9	0.0 / 0.3
	L3f	15	321	0.38	7.9	0	2.7 ± 2.4	2.5 ± 1.9	0.1 / 0.4
	L3g	250	30	0.39	0.2	0	-12.9 ± 5.8	-15.0 ± 6.1	2.1 /-0.3
	L3h	16	321	0.41	6.6	23	3.0 ± 3.5	3.1 ± 2.9	-0.2 / 0.6
	L3i	17	321	0.37	6.2	0	-3.1 ± 2.9	-2.8 ± 2.5	-0.3 / 0.4
	L3j	26	321	0.39	4.0	0	-3.3 ± 3.5	-2.9 ± 2.6	-0.4 / 0.8
	L3k	23	321	0.33	4.4	0	1.9 ± 3.0	2.4 ± 2.8	-0.5 / 0.2
	L2d			*no data*					
	L2e	250	18	0.34	0.1	0	-3.2 ± 7.0	-1.4 ± 7.7	-1.8 /-0.7
	L2f			*no data*					
Track 360	L2a	132	160	0.29	0.7	1	-11.4 ± 7.1	-11.8 ± 7.4	0.4 /-0.2
	L2b	16	309	0.32	7.4	0	0.9 ± 1.8	0.5 ± 1.9	0.4 / 0.0
	L2c	57	308	0.34	1.7	0	9.8 ± 4.1	9.6 ± 4.5	0.2 /-0.4
	L3a	13	309	0.32	9.3	33	-2.2 ± 2.1	-2.5 ± 2.2	0.3 /-0.1
	L3b	13	309	0.33	59.9	99	1.3 ± 2.4	0.9 ± 1.9	0.4 / 0.5
	L3c	13	308	0.32	16.8	100	-1.3 ± 2.2	-1.1 ± 1.9	-0.2 / 0.3
	L3d	13	309	0.32	14.7	98	0.6 ± 2.0	0.8 ± 1.8	-0.2 / 0.2
	L3e	26	308	0.38	12.6	71	0.9 ± 3.5	1.2 ± 3.0	-0.3 / 0.5
	L3f	250	309	0.39	2.8	100	-10.9 ± 4.3	-10.3 ± 4.3	-0.6 / 0.0
	L3g	128	233	0.40	8.1	74	-7.0 ± 7.3	-6.8 ± 7.4	-0.2 /-0.1
	L3h	80	308	0.40	7.1	100	-12.3 ± 3.2	-11.6 ± 2.9	-0.7 / 0.3
	L3i	17	309	0.38	6.2	0	-1.1 ± 2.6	-0.1 ± 2.6	-1.1 / 0.0
	L3j	40	309	0.37	4.9	2	1.4 ± 2.8	2.6 ± 2.7	-1.2 / 0.1
	L3k			*no data*					
	L2d	67	309	0.33	1.3	0	1.1 ± 3.9	2.9 ± 3.6	-1.8 / 0.4
	L2e	250	65	0.33	0.3	0	7.9 ± 6.7	12.1 ± 6.7	-4.2 / 0.0
	L2f			*no data*					

ICESat elevation errors for repeats of Tracks 85 and 360, listed in time order by campaign. The format is similar to that of Table III. Repeats where the gain value is shaded grey were part of the mission saturation calibration experiments and are explicitly excluded in some of the Table III results.

or imperfect knowledge of spacecraft orientation) whose effect would appear as uniform offsets between repeats. To estimate the precision of the ICESat elevation measurement, we removed the median elevation residual value from each repeat, then calculated the standard deviation of all median-adjusted footprints. We obtained a value of 2.8 cm, which is our estimate of ICESat elevation precision over any 50-km profile. The distribution of the demeaned residuals passed the K–S test for a Gaussian distribution at the 95% level, which is evidence that ICESat elevation error over distances of 50 km or less was generated by random white noise processes (e.g., laser range jitter).

Elevation precision varied considerably between repeats of a given track (Fig. 4, Table IV). Of the 30 ICESat repeats over the DEM, 11 had an elevation standard deviation of ≤ 2.5 cm (high precision) with respect to the DEM, while five had a standard deviation of ≥ 5.8 cm (low precision). We found that the difference in precision was related to energy and gain: the high-precision population had high-amplitude received energy and low values of the receiver gain; conversely, the low-precision population had low-amplitude received energies and high gain values. The 1.8-cm standard deviation achieved for L2b Track 85 and L3c/L3d Track 360 (Table IV) is our estimate of the best-case ICESat precision for a single repeat.

In summary, our definitive estimate of ICESat elevation accuracy for any randomly selected footprint in the data set is 0.0 cm (i.e., no bias with respect to our terrestrial reference), and our definitive estimate of precision for any single footprint

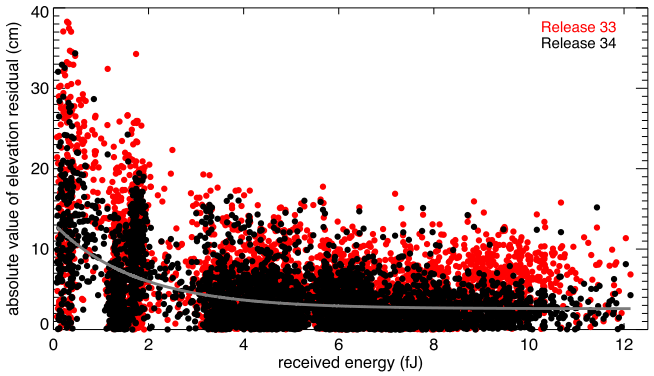

Fig. 5. Absolute value of the elevation residual (difference between ICESat elevations and reference elevations) versus received energy for Release 33 (red) and 34 (black) data, with exponential fit to Release 34 data (gray). Lower received energies yielded larger residuals, affecting performance under (for example) cloudy conditions or late in the operational life of a laser.

is 4.0 cm. We estimate ICESat elevation precision on any single 50-km profile to be 2.8 cm, improving to 1.8 cm under ideal conditions.

2) Ascending Versus Descending Tracks: The elevation error for all 4219 footprints on descending Track 85 was 0.0 ± 4.5 cm versus -0.7 ± 4.9 cm for the 4162 footprints on ascending Track 360. Excluding the saturation test campaigns reduced the error on Track 360 to 0.1 ± 3.8 cm (Table III), such that the resulting difference in bias (0.0 vs. 0.1 cm) was not significant at the 5% level (Appendix A1). These results are consistent with there being no bias between ICESat's ascending and descending tracks.

3) Relationship Between Receiver Gain and ICESat Elevation Quality: We examined the relationship between ICESat elevation accuracy/precision and receiver gain. The elevation error for the 4861 footprints with gain ≤ 20 ("low gain") was 0.0 ± 3.4 cm versus -6.2 ± 11.5 cm for the 1719 ICESat footprints with gain ≥ 50 ("high gain") (Table III). A similar relationship held when footprints were aggregated into individual repeats: the average bias for the 15 repeats acquired with a low gain was -0.5 ± 2.4 cm, whereas for the nine repeats acquired with high gain, the bias was -4.3 ± 5.5 cm (Table IV). The poor results at higher gain suggest that receiver gain is a rough proxy for the quality of ICESat elevations, with gain values less than $\sim$50 generally associated with better accuracy and precision.

The degradation of accuracy and precision for the high-gain footprints in our data set occurs for different reasons, which we illustrate by splitting the 1719 high-gain footprints into two populations: 795 footprints that were saturation corrected and 924 footprints that had no saturation correction.

For the 924 high-gain footprints with no saturation correction, the elevation error was 2.3 ± 10.3 cm (Table III). The poor 10.3-cm precision of these footprints is consistent with their exceptionally low 1.4-fJ average return energy, which resulted in a low signal-to-noise ratio at the ICESat detector (leftmost points in Fig. 5). Low return energies also explain the lack of a saturation correction for these footprints, since saturation only occurred when return energies were high enough to exceed the detector's dynamic range [46].

The elevation error for the 795 saturation-corrected high-gain footprints was -11.2 ± 4.7 cm (Table III), indicating similar precision to that of the entire data set, but a large negative bias. These 795 footprints were all associated with the saturation correction tests on the salar, during which the gain levels were artificially fixed to high values to induce detector saturation. Since the saturation correction increases elevations, the significant negative bias for these footprints indicates that the saturation correction value in the GLA06 data product is too small under conditions of high laser energy and high gain.

4) Investigation of Pointing Error and Forward Scattering: To test whether ICESat might have a systematic pointing bias, we examined the correlation between ICESat elevation residuals and off-nadir pointing angle. We did not find significant correlation; however, the small range of off-pointing angles in our data set (0.29–0.41°, Table IV) limits the diagnostic power of the analysis. It is also possible that the orientation of the pointing vector relative to the local instrument-centered coordinate system could have an effect on ICESat elevations, but our data set at the salar de Uyuni is not large enough to distinguish between the four different ICESat orientation directions.

In an earlier study [19], we found evidence for a negative elevation bias on L2a Track 360 due to forward scattering from clouds. Using true color Moderate Resolution Imaging Spectroradiometer (MODIS) reflectance imagery from NASA's Worldview tool (https://worldview.earthdata.nasa.gov), we searched for visible clouds over the salar de Uyuni on the dates of all 30 ICESat repeats. The only other repeats that we could associate with visible clouds within 12 h of the overflight time were L3g Track 85, which exhibited a similarly large negative elevation bias (-12.9 cm) and L2e Track 85 (-3.2 cm). All three repeats had exceptionally low return energy (< 1 fJ, Table IV). On analysis, we discovered we could use the ratio of transmit to return energy as a proxy for atmospheric transmission loss over the nearly uniform albedo salar. The three repeats we flagged for visible clouds also had a significantly lower return energy ratio than any of the other repeats. Given the limited number of repeats over Uyuni that were impacted by clouds, we did not attempt to further analyze the forward scattering bias.

B. Assessment of ICESat Elevation Quality Using the Repeat-Track Method

We repeated the analysis from Section III-A using the repeat-track method. For Tracks 85 and 360 over the Uyuni DEM, both the overall (Table III) and repeat-to-repeat (Table IV) elevation errors for the DEM and repeat-track methods were nearly identical, with just a few millimeters discrepancy between them. The differences between the biases from the two methods changed slightly but systematically between earlier and later campaigns (rightmost column in Table IV). Early campaigns tended to have DEM biases higher than repeat-track biases, with the situation reversed for later campaigns. There is no such pattern for the standard deviations. This result is consistent with the way we constructed the DEM reference elevations, whereby they consisted of a time-weighted linear combination of our 2002 and 2009 DEMs for

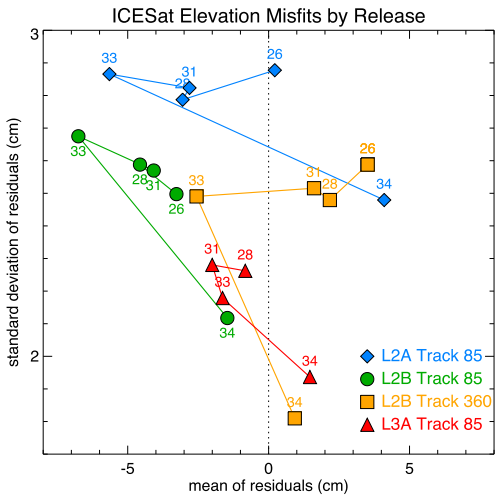

Fig. 6. Evolution of ICESat elevation errors (mean on x-axis, standard deviation on y-axis) by data release for four repeats obtained over the salar de Uyuni under clear sky conditions with moderate to high return energy. Releases are indicated by the small number next to the symbols (see Table II). Release 34 was the only release to show a large reduction in standard deviation of the residuals between ICESat and the Uyuni DEM.

each ICESat repeat, resulting in slightly different elevations over time. The repeat-track reference elevations track did not change with time, and the outcome was a small time-dependent difference between the DEM and repeat-track methods (right column of Table III).

C. Evolution of ICESat Elevation Observations Over Successive Data Releases

Improvements in ICESat data processing were systematically incorporated into data products through a series of data product releases (Section II-B, Table II). Releases 31, 33, and 34 were the only releases to include all data collected by the mission, and only Releases 33 and 34 are currently available through NSIDC. During the course of the mission, we archived data from prior releases, which we used for the analysis described below.

To illustrate how processing changes impacted ICESat geolocation, we calculated the elevation errors for ICESat footprints over the salar de Uyuni DEM for data releases 28 through 34, excluding footprints from the last four campaigns (L3k, L2d, L2e, L2f) since these were not processed for Release 28. We obtained values of 0.5 ± 6.7 cm (Release 28), 0.8 ± 7.3 cm (Release 31), -2.8 ± 5.5 cm (Release 33), and -0.6 ± 4.6 cm (Release 34). Although these results show that ICESat elevation accuracy for the data set as a whole did not improve between Releases 28 and 34, precision improved significantly.

In addition, we examined the errors for several repeats that took place under ideal conditions: medium-to-high transmit energy (high signal-to-noise ratio), no clouds (little or no forward scattering), and no standing water on the salar (no specular reflection of the return). For these high-quality repeats (campaigns L2a, L2b, and L3a on Track 85 and L2b on Track 360), the impact of processing changes between Releases 26 and 33 on the standard deviation (scatter) of the elevation residuals was minimal, not more than 0.2 cm for any of the repeats (Fig. 6). However, the mean of the elevation residuals (the bias) became progressively more negative between releases, with all biases having values less than zero in Release 33.

Release 34 was a major improvement over Release 33, resulting in a 10%–40% reduction in the scatter of the elevation residuals and a 10%–80% reduction in the absolute value of the elevation biases. Three of the four repeats had an elevation bias within 1.6 cm of zero. Of note, L2a Track 85 consistently showed larger scatter than the other three repeats. Although its parameters were well within the range covered by the saturation correction [46], some undetermined combination of spacecraft, instrument, and environmental factors impacted L2a Track 85 differently than the other high-quality repeats we examined.

D. ICESat Intercampaign and Interlaser Biases

1) ICB Values and Confidence Intervals: We estimated ICESat ICBs and their uncertainties (Appendix A2) from repeat-track elevation residuals for each ICESat campaign over the salar de Uyuni (Table V, Column 2). We omitted the five repeats along Track 360 that were used in the saturation tests, since these were unlikely to be representative of ICESat data under normal operating conditions.

For the salar de Uyuni, our estimated ICB values ranged from -4.2 to $+8.1$ cm. The 95% confidence interval on the ICBs included 0 m for all campaigns except L2f (whose uncertainty is undefined), indicating that the ICBs did not differ significantly from zero. Although our analysis includes only a few repeats (≤ 4) for each campaign, the magnitude and variability of our ICB values are similar to those from studies using more data over larger areas (see Section IV).

2) ICB Trends: Although our estimates of individual ICBs were not statistically significant, we considered the possibility that the ICBs in aggregate resulted in a systematic trend in ICESat elevations over the course of the mission. We estimated ICB trends over the salar de Uyuni from a weighted least-squares line fit to the ICB values, with inverse-variance weights calculated from the ICB uncertainties reported in Table V. We obtained a trend of 0.3 ± 0.4 (1σ) cm per year (Table V) for the period spanning campaigns L2a to L2e (omitting L2f, for which we had only one measurement and thus no error estimate). Based on the relevant t-test (Appendix A4), the trend is indistinguishable from zero at the 5% significance level

Since early ice mass balance studies using ICESat data did not have access to data from the entire mission, we also calculated ICB trends spanning successively shorter periods: between campaigns L2a and L2e, L2d, L3k, and L3j (Table V). The ICB trend for the salar de Uyuni shifted monotonically from positive to negative for progressively shorter time intervals, but in no case was the trend statistically significant.

3) Interlaser Bias: We also investigated whether there might be a systematic elevation bias between ICESat's two primary lasers: Laser 2 (which operated at the beginning and end of the mission, Table I) and Laser 3 (which operated in the middle of the mission). We estimated the bias by subtracting the mean of the ICBs for the 11 Laser 3 campaigns from the mean for the six Laser 2 campaigns, finding a positive 3.1-cm Laser 2 bias relative to Laser 3. This interlaser bias was significant at the 5% level (Appendix A3).

TABLE V
ICESAT ICBS, INTERCAMPAIGN TRENDS, AND INTERLASER BIAS

	This study	Hofton et al. (2013)		Richter et al. (2014)	Schröder et al. (2017)	Urban et al. (2013)	Zwally et al. (2015)
Campaign	salar de Uyuni	86° South	EA Divide	Vostok	EA Traverse	Ocean	Polar Sea-Ice
L2a	4.5 ± 5.4	3.2 ± 1.8	0.4 ± 5.5	2.1 ± 1.2	3.6 ± 0.9	4.8 ± 1.3	0.6
L2b	0.4 ± 1.5	-1.0 ± 4.3	-1.6 ± 4.3	-0.7 ± 1.1	-0.1 ± 0.9	0.5 ± 1.3	6.4
L2c	5.2 ± 4.1	7.1 ± 5.5	2.4 ± 5.7	6.3 ± 1.0	5.2 ± 0.8	4.1 ± 0.9	7.4
L3a	1.0 ± 3.0	-2.7 ± 4.0	-6.7 ± 3.9	-3.2 ± 0.9	-3.1 ± 0.9	1.0 ± 1.3	1.7
L3b	5.7 ± 6.5	-2.5 ± 3.1	-5.1 ± 4.6	-4.0 ± 0.9	-1.7 ± 0.8	0.2 ± 1.1	-0.6
L3c	1.6 ± 1.8	-3.6 ± 3.9	-6.2 ± 4.7	-2.9 ± 0.8	-2.1 ± 0.7	1.0 ± 1.5	2.3
L3d	0.0 ± 2.8	1.6 ± 2.5	-3.2 ± 4.2	0.4 ± 0.8	1.9 ± 0.7	0.4 ± 1.0	-3.7
L3e	-4.2 ± 2.8	1.8 ± 1.6	-1.1 ± 4.5	-1.1 ± 0.8	0.2 ± 0.7	0.3 ± 0.7	-0.1
L3f	1.7 ± 7.5	-2.2 ± 2.3	-4.9 ± 4.9	-1.7 ± 0.8	-1.0 ± 0.6	0.1 ± 0.9	-2.8
L3g	0.4 ± 5.8	3.2 ± 0.8	-1.1 ± 4.9	2.4 ± 0.8	2.4 ± 0.6	1.9 ± 0.7	-3.7
L3h	2.8 ± 3.8	1.2 ± 1.8	0.1 ± 3.0	-1.0 ± 0.8	0.0 ± 0.6	1.2 ± 0.9	1.4
L3i	0.0 ± 1.9	0.0 ± 3.2	0.0 ± 3.3	0.0 ± 0.9	0.0 ± 0.6	0.0 ± 0.9	-4.0
L3j	-3.3 ± 5.5	3.5 ± 2.3	1.3 ± 5.2	3.1 ± 1.0	2.5 ± 0.6	-1.2 ± 1.4	-3.0
L3k	3.1 ± 1.7	6.2 ± 2.6	3.1 ± 3.4	4.3 ± 1.2	3.7 ± 0.6	-0.7 ± 2.0	-2.2
L2d	3.7 ± 3.3	7.7 ± 1.5	7.3 ± 4.5	5.0 ± 1.2	5.9 ± 0.6	5.7 ± 1.7	-2.2
L2e	8.1 ± 6.3	14.7 ± 3.0	13.9 ± 4.9	5.6 ± 1.3	8.7 ± 0.6	11.2 ± 7.3	
L2f	1.3	7.4 ± 2.8	4.2 ± 4.4	4.2 ± 1.3	6.1 ± 0.6	4.9 ± 1.2	
trend L2a-L3j	-0.5 ± 0.6	0.3 ± 0.5	0.9 ± 0.9	0.2 ± 0.2	0.0 ± 0.1	**-0.7 ± 0.2**	**-1.9 ± 0.5**
trend L2a-L3k	0.1 ± 0.4	0.6 ± 0.4	1.2 ± 0.7	**0.5 ± 0.2**	**0.4 ± 0.1**	**-0.7 ± 0.2**	**-1.6 ± 0.4**
trend L2a-L2d	0.2 ± 0.4	**1.1 ± 0.4**	**1.5 ± 0.7**	**0.7 ± 0.2**	**0.7 ± 0.1**	-0.4 ± 0.2	**-1.4 ± 0.4**
trend L2a-L2e	0.3 ± 0.4	**1.4 ± 0.4**	**2.0 ± 0.6**	**0.8 ± 0.2**	**1.1 ± 0.1**	-0.4 ± 0.2	
trend L2a-L2f		**1.4 ± 0.3**	**1.9 ± 0.6**	**1.0 ± 0.1**	**1.2 ± 0.1**	0.0 ± 0.2	
Laser 2 mean	3.9	6.5	4.4	3.8	4.9	5.2	3.1
Laser 3 mean	0.8	0.6	-2.2	-0.3	0.3	0.4	-1.3
inter-laser bias	**3.1**	**5.9**	**6.6**	**4.1**	**4.6**	**4.8**	**4.4**
ex laser bias trend L2a-L3j	0.3 ± 0.6	**1.7 ± 0.5**	**2.1 ± 0.9**	**1.0 ± 0.2**	**0.9 ± 0.1**	0.4 ± 0.2	-0.9 ± 0.5
ex laser bias trend L2a-L3k	0.7 ± 0.4	**1.8 ± 0.4**	**2.2 ± 0.7**	**1.2 ± 0.2**	**1.1 ± 0.1**	0.4 ± 0.2	-0.8 ± 0.4
ex laser bias trend L2a-L2d	0.6 ± 0.4	**1.2 ± 0.4**	**2.0 ± 0.7**	**1.1 ± 0.2**	**0.9 ± 0.1**	0.4 ± 0.2	**-1.0 ± 0.4**
ex laser bias trend L2a-L2e	0.7 ± 0.4	**1.4 ± 0.4**	**2.2 ± 0.6**	**1.0 ± 0.2**	**1.0 ± 0.1**	0.4 ± 0.2	
ex laser bias trend L2a-L2f		**1.2 ± 0.3**	**1.8 ± 0.6**	**1.0 ± 0.1**	**0.9 ± 0.1**	0.3 ± 0.2	

(Top Section) Published estimates of ICESat intercampaign biases (ICBs) and their 1σ error estimates for various studies. Bias values are referenced to campaign L3i to aid intercomparison. (Upper middle section) ICB trends and trend uncertainties from each study's raw ICB data, colored blue for statistically significant positive trends and red for statistically significant negative trends. The five entries correspond to progressively longer timespans, as indicated by the starting and ending campaigns. (Lower middle section) Estimates of the mean ICBs for ICESat lasers and their difference. Positive inter-laser bias for Laser 2 is statistically significant for all studies. (Bottom section) Re-estimation of the ICB trends with the inter-laser bias removed.

Removing the interlaser bias from the ICBs and reestimating the ICB trends for all time intervals narrowed the range of the ICB trend estimates and shifted them all toward more positive values (Table V). As was the case with the original ICB trends, none of the reestimated trends on the salar de Uyuni were statistically significant.

E. Stability of the Salar de Uyuni Surface

To be useful for ICESat Cal/Val, the salar de Uyuni surface had to be stable in addition to being flat. From visual inspection of flooded Landsat and MODIS imagery [6], we knew qualitatively that the landforms in our Uyuni DEMs were permanent features of the surface on decadal timescales. More quantitatively and on shorter timescales, we assessed the stability of the salar de Uyuni surface in two ways. First, by directly differencing the 2002 and 2009 GPS DEMs (see [46]), we estimated topographic change over 7 years to have been 2.3 ± 3.4 cm (1σ), with maximum change of ± 10 cm in a few small areas. This overall uplift is only slightly greater than the contemporaneous 1.6 ± 3.6 cm elevation change we observe at eight fixed GPS sites within the DEM boundaries (locations in [9]). It is also consistent with an estimate of local isostatic crustal rebound of 27 m over the past 14–17 kyr in response to the evaporation of paleolake Minchin [5].

We also independently estimated vertical motion within the GPS DEM boundary using InSAR. From an InSAR pair between August 24, 2009 and August 27, 2010 (1 year) (Fig. 3), we estimated the vertical motion of the salar surface within the GPS DEM boundary to have been 0.0 ± 0.7 cm (1σ). From a similar analysis of interferograms from August 27, 2010 to January 12, 2011 (6 months, winter to summer) and October 4, 2007 to August 27, 2010 (3 years), we estimated vertical motion to be, respectively, 0.0 ± 0.6 cm and 0.0 ± 1.2 cm. Since InSAR only measures relative elevation changes within an interferogram, the zero mean change within the DEM boundaries is consistent with long-wavelength uplift affecting both the salar de Uyuni and environs, which is what we would expect from a broad isostatic rebound signal.

Together these results suggest that the surface is stable at the subcentimeter level on seasonal/annual timescales and at the several centimeter level over timescales of up to 7 years, with expected secular uplift of ∼2 mm per year from isostatic rebound.

IV. DISCUSSION

A. ICESat Accuracy and Precision

Analyzing all ICESat elevations acquired over the salar, we found no systematic bias with respect to the Uyuni DEM and no evidence of a mission-wide ascending versus descending orbit bias, which has been an issue for other altimeters [31], [32]. Since our results are confined to one geographic location, they are consistent with there being zero

biases everywhere along ICESat's orbit, but we note that they cannot definitely establish that this is the case.

Individual repeats did exhibit significant biases with respect to the Uyuni DEM (Table IV), but differences between repeats were expected and were not the primary focus of this paper. Notably, for gain values > 50, we observed a $+2$-cm bias for unsaturated footprints and a -11-cm bias for saturated footprints, suggesting that there may be systematic uncalibrated effects at higher gain values. Accordingly, ICESat data users should consider differences in gain values when interpreting small changes in elevations.

We observed elevation variability of 1.8 cm (1σ) for individual repeats under ideal conditions, which we consider to be the precision limit of ICESat elevation measurements along relatively short (50 km) segments of the satellite ground track. Aggregating all repeats over the salar, the elevation variability increased to 2.8 cm (1σ), which is comparable to the best individual repeats observed in [19] and the single-repeat 2.5-cm standard deviation reported in [2]. Since those earlier studies only considered data through Release 22, our results appear to reflect significantly improved processing between Releases 22 and 34. In all cases, the elevation measurement performance far exceeded the <10-cm single-footprint ranging accuracy expected prior to launch [1].

For all ICESat data over the salar, we estimated an ICESat elevation precision of 4.0 cm (1σ), which reflects noise on individual tracks plus track-to-track biases from errors in orbit determination and spacecraft orientation. Precision degraded with lower received energy, particularly when energy dropped below $\sim$3 fJ (Fig. 5). These low energies resulted in higher gain values, with gain > 50 associated with significantly lower accuracy and precision than the data set as a whole. This underscores the negative effect of declining laser transmit energy over the life of each laser (Table I), which directly translated to lower received energy. Although lower received energy triggered an automatic increase in detector gain to allow the instrument to detect the ground-reflected pulse, the increased gain magnified both the signal and the noise received by the ICESat detector and thus did not improve the signal-to-noise ratio for low-energy returns.

We did not find evidence for ICESat pointing biases in our data set, although we cannot rule out biases that would show up with larger off-pointing angles (e.g., those associated with ICESat TOOs), and we do not have sufficient data to analyze the possible impact of the pointing vector orientation relative to the spacecraft. We did confirm earlier findings of a centimeter-to-decimeter negative elevation bias from forward scattering [12], [19], but we did not have enough cloud-impacted data over the salar de Uyuni to model this effect.

B. Saturation Correction Under High-Gain/ High-Energy Condition

A new finding of this paper is that the ICESat saturation correction appears to undercorrect elevations derived from footprints associated with high gain and high energy. We expect such footprints to have been infrequent, occurring primarily in the short interval after the transition of the ICESat ground track from a low-albedo to high-albedo surface (e.g., from ocean to ice), before ICESat's automatic gain control loop could adjust the gain downward. The first shots on a high-albedo surface after such a transition could be strongly saturated, yielding anomalously low elevations that are not fully corrected. This behavior may be of interest to investigators working on sea ice, ice shelves, or the ice sheet margins, whose results would be adversely affected by decimeter-level negative elevation biases near the ice periphery.

C. Comparisons of ICESat Data Releases

The ICESat mission presented an unusual calibration and validation challenge due to the number and pace of data product releases throughout the mission. Multiple new versions of the GLAS Science Algorithm Software (GSAS) were delivered each year, with a new data product release accompanying each software version (Table II, https://nsidc.org/data/icesat/isips_release.html). Although only selected releases were made publicly available, our team analyzed data from almost all of the 18 releases listed in Table II and from a few that did not make the official list (e.g., releases 16, 20, and 23). Our main objective for most releases was to ensure that there was no major problem with the processing, but we also traced the evolution of geolocation for some early ICESat observations through the entire release chain.

Our results for the most recent five data releases (Fig. 6) show the significant improvement in elevation bias and standard deviation that occurred in the final release 34 data set. Since early mission publications necessarily used early-release ICESat data, there is a potential benefit to revisiting those studies using data processed to current standards. Investigators referencing early ICESat publications should be appropriately cautious about results that rely on small elevation changes (order several centimeters or less) unless these results have been subsequently confirmed using Release 34 data.

D. Intercampaign Biases

ICB is an ICESat-specific term which was introduced to describe unexplained systematic differences between mean elevations acquired during different campaigns [22]. Although estimated ICBs can be large enough to change the sign of ICESat-derived ice sheet surface mass balance [57], the wide range of ICB estimates from different sources [49] raises questions about the utility of ICBs as a potential correction for ICESat elevations [10].

We analyzed ICBs from the salar de Uyuni (Table V, Column 2) together with ICBs from recently published studies (Table V, Column 3–8) over the global oceans [39], [49], the Antarctic interior [23], Lake Vostok [36], and leads in polar sea ice (D_{SL} from [57]). For ease of comparison, we obtained the ICBs associated with these studies from the NSIDC website (https://nsidc.org/icesat/guide-applying-icesat-inter-campaign-bias-corrections-icbs), which provides G$-$C corrected ICBs for the studies based on Release 33 data. The ICBs for each study were referenced to campaign L3i, which was assigned a value of zero.

The salar de Uyuni ICBs ranged from -4.2 to 8.1 cm and had a standard deviation of 3.1 cm, which was consistent with, but on the low end of, the other ICB estimates (Table V).

None of the Uyuni ICBs were statistically distinguishable from zero, which was not unexpected given the small number of repeats over the salar de Uyuni and the correspondingly wide confidence intervals. Conversely, the much larger number of repeats analyzed in the other studies (ranging from a low of 18 repeats in [36] up to many hundreds) yielded statistically significant ICBs for most campaigns in most studies.

Although this result suggests that more data might have yielded significant ICBs at Uyuni, the underlying problem with the other published ICB estimates we analyzed is that they are largely incompatible with each other. For instance, the 95% confidence intervals of the [49] ICB estimates: 1) do not overlap with those of any other study for 11 of 17 campaigns and 2) only overlap with those of one other study for 4 of the other 5 campaigns. This suggests either a flaw in the assumption that ICBs are uniform at the global scale or overoptimistic ICB uncertainty estimates. In the first case, if ICBs have a location dependence (as would occur if there were orbit-dependent errors in spacecraft positioning or pointing), then it is possible that ICBs for a given campaign would be statistically different in different studies. In the second case, if estimated uncertainties are too small, then the range of possible ICB values around the chosen value will be too narrow and will not properly overlap the range of other studies' ICBs. In either case, the lack of consensus between these studies makes us hesitant to recommend using any set of ICBs to correct elevations from individual ICESat campaigns.

E. Intercampaign Bias Trends

Trends in the ICB estimates over time provide insights into possible systematic errors that would affect the ICESat elevation series. Since small surface elevation changes over Earth's ice sheets can have large impacts on mass loss estimates from altimetry, this is an important topic for ICESat Cal/Val [29].

For the salar de Uyuni, ICB trend values were consistently small for all timespans, and none differed significantly from zero (Table V, Column 2). To provide a broader context for the Uyuni results, we estimated ICB trends for the studies cited above using their reported ICBs and uncertainties (Table V). For the four estimates over Antarctica (Table V, Columns 3–6), the trend is positive for all timespans and is both strongly positive (>1 cm per year) and statistically significant for most of the longer timespans. The global ocean estimate (Table V, Column 7) is zero or modestly negative for all timespans and is statistically significant for shorter timespans. The polar sea-ice estimate (Table V, Column 8), for which we assume a uniform 2.4-cm standard error (i.e., the average uncertainty for all ICBs in all cited studies), is strongly and significantly negative. As with the ICBs themselves, these trend estimates are inconsistent and in many cases statistically incompatible with each other.

F. Interlaser Bias

Although we did not find evidence for ICBs or ICB trends in salar de Uyuni data, we did find a statistically significant 3.1-cm elevation bias between Laser 2 and Laser 3, which has not been previously reported. We found a similar interlaser bias in data from the other studies we examined (Table V), with the Uyuni estimate on the low end of the range.

We can identify two potential sources of interlaser bias: 1) since the outgoing laser pulse for each laser initially followed a different optical path, it is possible that the accompanying interlaser timing biases were not fully calibrated; and 2) observed differences in footprint size/ellipticity between lasers may have contributed to a systematic bias in elevation estimation due to different elevation sampling within the footprint. Analysis of the contributing factors to the interlaser bias is an avenue for future study.

Removing the interlaser bias from the ICBs and reestimating ICB trends improved the consistency of the ICB trend estimates across various timespans for all studies and shifted the ICB trends toward more positive values [Table V (bottom)]. With the interlaser bias removed, the one global analysis [62] agrees with our findings that there are no significant ICB trends in ICESat elevations. In the four Antarctica studies, the new ICB trends are more positive overall and all are statistically significant. The work in [57] remains an outlier with its negative and statistically significant ICB trends for various timespans, but the trend values are more consistent and less negative than before.

We recommend that investigators working with ICESat elevations consider removing an interlaser bias of 4.8 cm (the mean of the seven studies in Table V) from their data. For this correction, we suggest subtracting 2.9 cm from all Laser 2 campaigns and adding 1.9 cm to all Laser 3 campaigns, which is consistent with the partitioning of the bias between lasers in our comparison of pooled elevations at the salar de Uyuni (second set of entries in Table III).

G. Repeat-Track Versus DEM Validation

A primary innovation of this paper was comparing altimeter validation results from a terrestrial DEM (the DEM method) with those from the topographic profile derived by averaging the altimeter elevations themselves (the repeat-track method) and showing that the two methods produced nearly identical results. This is a significant finding, because the repeat-track method presents a much simpler alternative to traditional Cal/Val surveys in support of altimetry missions, bypassing the time-consuming logistics and costs associated with accessing and surveying a large reference surface such as the salar de Uyuni.

There are several limitations of using the repeat-track method for validation: 1) in the form we discuss here (which can be modified to mitigate this concern), it is limited to missions that collect data along a reference ground track, and it performs better the closer the altimeter footprints are steered toward that track. This is ideal for a repeat-track mission like ICESat-2, but not for a mission like CryoSat-2, whose track is allowed to drift over time; 2) more repeats along a given reference track yield better reference profiles, especially in the presence of noise. This limitation is most relevant early in a mission, but if the first phase of the mission is flown in a short-period repeat orbit, sufficient data can be collected in a few months to perform an initial validation; 3) absolute elevation accuracy with respect to the global reference frame has to be estimated using another method.

Despite these limitations, the repeat-track method has two key advantages: it eliminates the cost of *in situ* surveying and

it can be implemented over any flat surface (e.g., the Simpson Desert in Australia or the Etosha Pan in Namibia). In fact, the greatest benefit from the method would likely come from implementing it together with at least one independently surveyed DEM. A single DEM can provide absolute elevation validation, but it is limited both in terms of the number of ground tracks that intersect it and the fact that it samples only one location along the orbit. The addition of validation sites that span a range of latitudes would enable the characterization of errors that vary along the satellite orbit in both time and space.

V. Summary

We have compared ICESat data with GPS data acquired over the salar de Uyuni to provide new assessments of the accuracy and the precision of ICESat elevations. Our results are not definitive estimates of ICESat performance globally, but they do provide a benchmark for comparison with other studies and confirm that ICESat performance under ideal conditions significantly exceeded the mission design specifications. Our findings are as follows.

ICESat Accuracy and Precision: Our estimate of the ICESat Release 34 absolute elevation bias over the entire mission period is 0.0 cm. Our estimate of ICESat elevation precision ranges from 1.8 cm for single repeats under ideal conditions to 4.0 cm for all data under all conditions.

ICB: We did not find statistically significant ICESat ICBs or ICB trends. Our analysis of ICBs and trends for other published studies shows that although those estimates are statistically significant, and they are also statistically incompatible with each other. This suggests either that the estimated ICB uncertainties are too small or that the assumption of globally consistent ICBs is incorrect.

Interlaser Bias: There is strong evidence for a systematic bias between ICESat's lasers. Unlike individual ICBs, whose source is unknown by definition, this interlaser bias is associated with a specific ICESat subsystem whose parameters (e.g., optical alignment, footprint size, and shape) are known to vary between the three units on the spacecraft [2].

Comparison of Releases: ICESat performance improved over time with subsequent data releases, and the final Release 34 data set represents the highest quality ICESat elevation data produced for the mission.

High-Energy/High-Gain Footprint Bias: Footprints with high gain and high energy, such as those expected at transitions between open water and ice, may be negatively biased by 10 cm or more. More generally, footprints in the ICESat data set with gain > 50 should be used with care, since they exhibit significant saturation-dependent biases.

Validation Procedure: It is viable to perform terrestrial Cal/Val with averaged altimetry elevation profiles as a reference, potentially expanding the scope of altimeter validation to flat and stable terrestrial surfaces that have not been independently surveyed. This has important implications for Cal/Val of future satellite altimeter missions, since it limits the need for costly ground-based surveys. Our vision for the future of satellite altimeter Cal/Val is not just one or two expensive DEMs, but a network of individual sites that together form a single virtual reference surface spanning the globe.

Appendix

A. Test for Significance of Elevation Differences Between Descending Track 85 and Ascending Track 360

Based on numbers from Table III, we use the two-sample t-test for independent random samples to compare the elevation residual means between Track 85 ($\mu_1 = 0.0$ cm, $N_1 = 4219$, $s_1 = 4.5$ cm) and Track 360 ($\mu_2 = 0.1$ cm, $N_2 = 2695$, $s_2 = 3.5$ cm). We test the null hypothesis that $\mu_1 = \mu_2$ using the test statistic [37, Sec. 3.6.1]

$$t = \frac{|\mu_1 - \mu_2|}{\sqrt{\left(\frac{N_1+N_2}{N_1 N_2}\right)\left(\frac{(N_1-1)s_1^2+(N_2-1)s_2^2}{N_1+N_2-2}\right)}} \tag{A1}$$

with $N_1 + N_2 - 2 = 6912$ degrees of freedom, a significance level α of 5%, and a corresponding critical value $t_{\infty,\alpha=0.05} = 1.960$. Since $t = 1.054 < 1.960$, we cannot reject the hypothesis that the means are equal at a significance level of 5%

B. Intercampaign Bias Value and Confidence Interval Estimation

We estimated the ICB for a given campaign from the elevation residual medians $\tilde{r}_i$ of several repeats during that campaign (where $\tilde{r}_i$ are the values of the squares, triangles, etc., in Fig. 4). Specifically, the ICB is the weighted arithmetic mean of $\tilde{r}_i$ for all N repeats in a campaign, where the weights are the inverse sample variances s_i^2 of the scatter of elevation residuals about $\tilde{r}_i$

$$\text{ICB} = \frac{\sum_{i=1}^{N} \tilde{r}_i / s_i^2}{\sum_{i=1}^{N} 1/s_i^2} \tag{A2}$$

For the error on the ICBs, we calculated the inverse variance-weighed standard deviation s_{ICB} of the repeat medians about their ICB value using the unbiased estimator [20]

$$s_{\text{ICB}} = \sqrt{\frac{\sum_{i=1}^{N} (\tilde{r}_i - \text{ICB})^2 / s_i^2}{W_1 - W_2/W_1}} \tag{A3}$$

where

$$W_1 = \sum_{i=1}^{N} 1/s_i^2 \tag{A4}$$

$$W_2 = \sum_{i=1}^{N} \left(1/s_i^2\right)^2. \tag{A5}$$

Finally, we calculated the confidence intervals on the ICBs (Table V, Column 4) as

$$\pm \frac{t_{N-1,\alpha}\, S}{\sqrt{N}} \tag{A6}$$

using the t-statistic value $t_{N-1,\alpha}$ for significance level $\alpha = 5\%$ [37, Sec. 3.2]. The use of t-statistic requires that the underlying distribution does not deviate significantly from Gaussian, and we confirmed that the 17 ICB values for release 33 are Gaussian distributed at a significance level of 5%, based on the results of a standard K–S test. The release 34 ICBs do not meet the 5% standard, but their K–S significance (21%) indicates that they are sufficiently Gaussian for the application of statistical t-tests.

C. Tests for Significance of Elevation Differences Between Laser 2 and Laser 3

Using numbers from Table V, we employed the two-sample t-test (A1) to compare the ICB means between Laser 2 and Laser 3 for each of the studies shown. We tested the null hypothesis that $\mu_{\text{Laser2}} = \mu_{\text{Laser3}}$, with $N_2 = 6$ and $N_3 = 11$ degrees of freedom, a significance level α of 5%, and corresponding critical value $t_{15,\alpha=0.05} = 2.131$. In all cases, the estimated value of t exceeded 2.131, indicating that the interlaser bias was significant at the 5% level

D. Test for Significance of ICB Trend

To test whether the ICB trend differed significantly from zero, we employed student's t-test using the test statistic [37, Sec. 5.5.4]

$$t = \frac{|\beta|}{\sigma_\beta} \tag{A7}$$

where β is the trend value from the inverse-variance-weighted least-squares line fit and σ_β is the standard deviation of β derived from the fit. We chose a common significance level α of 5%, but each timespan in Table V had a different number of data N and thus a different critical value $t_{N-2,\alpha}$. For L2a to L2f, $N = 17$ and $t_{15,\alpha=0.05} = 2.131$. Similarly, for L2a to L2e, $t_{14,\alpha=0.05} = 2.145$; for L2a to L2d, $t_{13,\alpha=0.05} = 2.160$; for L2a to L3k, $t_{12,\alpha=0.05} = 2.179$; and for L2a to L3j, $t_{11,\alpha=0.05} = 2.201$. In cases where the test statistic t exceeded these critical values, we concluded that the trend was significant and reported this in Table V.

References

[1] J. B. Abshire *et al.*, "Geoscience laser altimeter system (GLAS) on the ICESat mission: Pre-launch and on-orbit measurement performance," in *Proc. IEEE Int. Geosci. Remote Sens. Symp.*, vol. 3, Jul. 2003, pp. 1534–1536.

[2] J. B. Abshire *et al.*, "Geoscience laser Altimeter system (GLAS) on the ICESat mission: On-orbit measurement performance," *Geophys. Res. Lett.*, vol. 32, no. 21, Nov. 2005, Art. no. L21S02. doi: 10.1029/2005GL024028.

[3] R. S. Afzal *et al.*, "Space qualification of the geoscience laser Altimeter system (glas) laser transmitters," Summaries Papers Presented at the Lasers Electro-Optics, Washington, DC, USA, 2002.

[4] Z. Altamimi, X. Collilieux, J. Legrand, B. Garayt, and C. Boucher, "ITRF2005: A new release of the international terrestrial reference frame based on time series of station positions and earth orientation parameters," *J. Geophys. Res.*, vol. 112, Sep. 2007, Art. no. B09401. doi: 10.1029/2007JB004949.

[5] B. G. Bills *et al.*, "Hydro-isostatic deflection and tectonic tilting in the central Andes: Initial results of a GPS survey of Lake Minchin shorelines," *Geophys. Res. Lett.*, vol. 21, no. 4, pp. 293–296, Feb. 1994.

[6] B. G. Bills, A. A. Borsa, and R. L. Comstock, "MISR-based passive optical bathymetry from orbit with few-cm level of accuracy on the salar de Uyuni, Bolivia," *Remote Sens. Environ.*, vol. 107, nos. 1–2, pp. 240–255, Mar. 2007.

[7] A. A. Borsa, J.-B. Minster, B. G. Bills, and H. A. Fricker, "Modeling long-period noise in kinematic GPS applications," *J. Geodesy*, vol. 81, no. 2, pp. 157–170, Feb. 2007. doi: 10.1007/s00190-006-0097-x.

[8] A. A. Borsa, B. G. Bills, and J.-B. Minster, "Modeling the topography of the salar de Uyuni, Bolivia, as an equipotential surface of Earth's gravity field," *J. Geophys. Res., Solid Earth*, vol. 113, no. B10, Oct. 2008, Art. no. B10408. doi: 10.1029/2007JB005445.

[9] A. A. Borsa, H. A. Fricker, B. G. Bills, J.-B. Minster, C. C. Carabajal, and K. J. Quinn, "Topography of the salar de Uyuni, Bolivia from kinematic GPS," *Geophys. J. Int.*, vol. 172, no. 1, pp. 31–40, Jan. 2008. doi: 10.1111/j.1365-246X.2007.03604.x.

[10] A. A. Borsa and G. Moholdt, H. A. Fricker, K. M. Brunt, "A range correction for ICESat and its potential impact on ice-sheet mass balance studies," *Cryosphere*, vol. 8, no. 2, pp. 345–357. 2014. doi: 10.5194/tc-8-345-2014.

[11] W. Bosch, D. Dettmering, and C. Schwatke, "Multi-mission cross-calibration of satellite altimeters: Constructing a long-term data record for global and regional sea level change studies," *Remote Sens.*, vol. 6, no. 3, pp. 2255–2281, Mar. 2014.

[12] A. C. Brenner, J. P. DiMarzio, and H. J. Zwally, "Precision and accuracy of satellite radar and laser altimeter data over the continental ice sheets," *IEEE Trans. Geosci. Remote Sens.*, vol. 45, no. 2, pp. 321–331, Feb. 2007.

[13] R. L. Brooks, W. J. Campbell, R. O. Ramseier, H. R. Stanley, and H. J. Zwally, "Ice sheet topography by satellite altimetry," *Nature*, vol. 274, pp. 539–543, Aug. 1978.

[14] C. H. Davis, C. A. Kluever, and B. J. Haines, "Elevation change of the southern Greenland ice sheet," *Science*, vol. 279, no. 5359, pp. 2086–2088, Mar. 1998.

[15] M. R. Drinkwater, R. Francis, G. Ratier, and D. J. Wingham, "The European space agency's earth explorer mission CryoSat: Measuring variability in the cryosphere," *Ann. Glaciology*, vol. 39, no. 1, pp. 313–320, 2004.

[16] S. Ekholm, R. Forsberg, and J. M. Brozena, "Accuracy of satellite altimeter elevations over the Greenland ice sheet," *J. Geophys. Res., Oceans*, vol. 100, no. C2, pp. 2687–2696, Feb. 1995.

[17] (Apr. 2013). *ESRIN—ESA and Mullard Space Science Laboratory—University College London Cryosat Product Handbook*. Accessed: Mar. 24, 2014. [Online]. Available: https://earth.esa.int/documents/10174/125272/CryoSat_Product_Handbook

[18] D. Felikson *et al.*, "Comparison of elevation change detection methods from icesat altimetry over the Greenland ice sheet," *IEEE Trans. Geosci. Remote Sens.* vol. 55, no. 10, pp. 5494–5550, Oct. 2017. doi: 10.1109/TGRS.2017.2709303.

[19] H. A. Fricker, A. Borsa, B. Minster, C. Carabajal, K. Quinn, and B. Bills, "Assessment of ICESat performance at the salar de Uyuni, Bolivia," *Geophys. Res. Lett.*, vol. 32, no. 21, Nov. 2005, Art. no. L21S06. doi: 10.1029/2005GL023423.

[20] M. Galassi *et al. GNU Scientific Library Reference Manual (3rd Ed.), Release 2.4*. [Online]. Available: https://www.gnu.org/software/gsl/

[21] N. Galin, D. J. Wingham, R. Cullen, M. Fornari, W. H. F. Smith, and S. Abdalla, "Calibration of the CryoSat-2 interferometer and measurement of across-track ocean slope," *IEEE Trans. Geosci. Remote Sens.*, vol. 51, no. 1, pp. 57–72, Jan. 2013. doi: 10.1109/TGRS.2012.2200298.

[22] B. Gunter *et al.*, "A comparison of coincident GRACE and ICESat data over Antarctica," *J. Geodesy*, vol. 83, pp. 1051–1060, Nov. 2009. doi: 10.1007/s00190-009-0323-4.

[23] M. A. Hofton, S. B. Luthcke, and J. B. Blair, "Estimation of ICESat intercampaign elevation biases from comparison of lidar data in East Antarctica," *Geophys. Res. Lett.*, vol. 40, no. 21, pp. 5698–5703, Nov. 2013.

[24] J. Kohler, T. A. Neumann, J. W. Robbins, S. Tronstad, and G. Melland, "ICESat elevations in Antarctica along the 2007–09 Norway–USA traverse: Validation with ground-based GPS," *IEEE Trans. Geosci. Remote Sens.*, vol. 51, no. 3, pp. 1578–1587, Mar. 2013. doi: 10.1109/TGRS.2012.2207963.

[25] N. T. Kurtz, N. Galin, and M. Studinger, "An improved CryoSat-2 sea ice freeboard and thickness retrieval algorithm through the use of waveform fitting," *Cryosphere Discuss.*, vol. 8, no. 4, pp. 1217–1237, 2014. doi: 10.5194/tcd-8-721-2014.

[26] S. Labroue, F. Boy, N. Picot, M. Urvoy, and M. Ablain, "First quality assessment of the Cryosat-2 altimetric system over ocean," *Adv. Space Res.*, vol. 50, no. 8, pp. 1030–1045, Oct. 2012. doi: 10.1016/j.asr.2011.11.018.

[27] S. B. Luthcke, D. D. Rowlands, T. A. Williams, and M. Sirota, "Reduction of ICESat systematic geolocation errors and the impact on ice sheet elevation change detection," *Geophys. Res. Lett.*, vol. 32, no. 21, Nov. 2005, Art. no. L21S05. doi: 10.1029/2005GL023689.

[28] L. A. Magruder, C. E. Webb, T. J. Urban, E. C. Silverberg, and B. E. Schutz, "ICESat altimetry data product verification at White Sands Space Harbor," *IEEE Trans. Geosci. Remote Sens.*, vol. 45, no. 1, pp. 147–155, Jan. 2007.

[29] A. Martin-Español, J. L. Bamber, and A. Zammit-Mangion, "Constraining the mass balance of east Antarctica," *Geophys. Res. Lett.*, vol. 44, no. 9, pp. 4168–4175, May 2017.

[30] D. D. McCarthy and G. Petit, "IERS Conventions," IERS Tech. Note 32, Jan. 2004.

[31] D. A. Mitchell, W. J. Teague, and K. R. Whitmer, "Evidence that Sea State bias is different for ascending and descending tracks," *Mar. Geodesy*, vol. 27, nos. 3–4, pp. 483–494, Jun. 2004.

[32] M. Naeije, E. Schrama, and R. Scharroo, "Calibration and validation of CryoSat-2 low resolution mode data," in *Proc. CryoSat Validation Workshop*, Feb. 2011, pp. 1–3.

[33] H. A. Phillips, G. Hyland, P. Morgan, R. Coleman, and N. Young, "Comparison of ERS altimeter and GPS heights on the Amery ice shelf, east Antarctica," in *Proc. 3rd ERS Symp. Space Service Environ.*, 1997, pp. 899–904.
[34] H. D. Pritchard, R. J. Arthern, D. G. Vaughan, and L. A. Edwards, "Extensive dynamic thinning on the margins of the Greenland and Antarctic ice sheets," *Nature*, vol. 461, no. 7266, pp. 971–975, Sep. 2009.
[35] J. Reuder, F. Ghezzi, E. Palenque, R. Torrez, and M. Andrade, "Investigations on the effect of high surface albedo on erythemally effective UV irradiance: Results of a campaign at the salar de Uyuni, Bolivia," *J. Photochem. Photobiol. B, Biol.*, vol. 87, no. 1, pp. 1–8, Apr. 2007. doi: 10.1016/j.jphotobiol.2006.12.
[36] A. Richter *et al.*, "Height changes over subglacial lake Vostok, East Antarctica: Insights from GNSS observations," *J. Geophys. Res., Earth Surf.*, vol. 119, no. 11, pp. 2460–2480, Nov. 2014.
[37] L. Sachs, *Applied Statistics: A Handbook of Techniques*. New York, NY, USA: Springer-Verlag, 1982.
[38] D. Sandwell, R. Mellors, X. Tong, M. Wei, and P. Wessel, "Open radar interferometry software for mapping surface deformation," *Eos Trans. AGU*, vol. 92, no. 28, p. 234, Jul. 2011. doi: 10.1029/2011EO280002.
[39] T. Scambos and C. Shuman, "Comment on 'Mass gains of the antarctic ice sheet exceed losses,'" *J. Glaciology*, vol. 62, no. 233, pp. 599–603, 2016.
[40] L. Schröder *et al.*, "Validation of satellite altimetry by kinematic GNSS in central East Antarctica," *Cryosphere*, vol. 11, pp. 1111–1130, May 2017.
[41] B. E. Schutz, H. J. Zwally, C. A. Shuman, D. Hancock, and J. P. DiMarzio, "Overview of the ICESat mission," *Geophys. Res. Lett.*, vol. 32, Art. no. L21S01, Nov. 2005. doi: 10.1029/2005GL024009.
[42] A. Shepherd *et al.*, "A reconciled estimate of ice-sheet mass balance," *Science*, vol. 338, no. 6111, pp. 1183–1189, Nov. 2012. doi: 10.1126/science.1228102.
[43] A. Shepherd *et al.*, "Mass balance of the Antarctic Ice Sheet from 1992 to 2017," *Nature*, vol. 556, pp. 219–222, Jun. 2018.
[44] C. A. Shuman *et al.*, "ICESat Antarctic elevation data: Preliminary precision and accuracy assessment," *Geophys. Res. Lett.*, vol. 33, no. 7, Apr. 2006, Art. no. L07501. doi: 10.1029/2005GL025227.
[45] M. R. Siegfried and R. L. Hawley, J. F. Burkhart, "High-resolution ground-based GPS measurements show intercampaign bias in ICESat elevation data near summit, Greenland," *IEEE Trans. Geosci. Remote Sens.*, vol. 49, no. 9, pp. 3393–3400, Sep. 2011. doi: 10.1109/TGRS.2011.2127483.
[46] X. Sun *et al.*, "ICESAT/GLAS altimetry measurements: Received signal dynamic range and saturation correction," *IEEE Trans. Geosci. Remote Sens.*, vol. 55, no. 10, pp. 5440–5454, Oct. 2017.
[47] T. J. Urban and B. E. Schutz, "ICESat sea level comparisons," *Geophys. Res. Lett.*, vol. 32, no. 23, Dec. 2005, Art. no. L23S10. doi: 10.1029/2005GL024306.
[48] T. Urban, S. Bae, H.-J. Rim, C. Webb, S. Yoon, and B. Schutz. (2011). CSR SCF Release Notes for Orbit and Attitude Determination, from ICESat/GLAS Data, Description of Data Releases. National Snow and Ice Data Center. [Online]. Available: https://nsidc.org/data/icesat/data_releases.html
[49] T. Urban *et al.*, " Summary of ICESat-1 intercampaign elevation biases and detection methods," in *Proc. Fall Meeting*, San Francisco, CA, USA, Dec. 2012, pp. 3–7.
[50] G. Wadge and D. J. Archer, "Evaporation of groundwater from arid playas measured by C-band SAR," *IEEE Trans. Geosci. Remote Sens.*, vol. 41, no. 7, pp. 1641–1650, Jul. 2003.
[51] C. E. Webb, Z. H. Jay, and W. Abdalati, "The Ice, cloud, and land elevation satellite (ICESat) summary mission timeline and performance relative to pre-launch mission success criteria," NASA, Washington, DC, USA, Tech. Rep. NASA/TM-2013-217512, 2013.
[52] D. J. Wingham, A. J. Ridout, R. Scharroo, R. J. Arthern, and C. K. Shum, "Antarctic elevation change from 1992 to 1996," *Science*, vol. 282, no. 5388, pp. 456–458, Oct. 1998.
[53] D. J. Wingham *et al.*, "CryoSat: A mission to determine the fluctuations in Earth's land and marine ice fields," *Adv. Space Res.*, vol. 37, no. 4, pp. 841–846, 2006.
[54] C. Zelli and A. Aerospazio, "ENVISAT RA-2 advanced radar altimeter: Instrument design and pre-launch performance assessment review," *Acta Astronautica*, vol. 44, no. 7, pp. 323–333, Apr./Jun. 1999.
[55] H. J. Zwally, R. A. Bindschadler, A. C. Brenner, J. A. Major, and J. G. Marsh, "Growth of Greenland ice sheet: Measurement," *Science*, vol. 246, no. 4937, pp. 1587–1589, Dec. 1989.
[56] H. J. Zwally *et al.*, "ICESat's laser measurements of polar ice, atmosphere, ocean, and land," *J. Geodyn.*, vol. 34, nos. 3–4, pp. 405–445, Oct./Nov. 2002.
[57] H. J. Zwally, J. Li, J. W. Robbins, J. L. Saba, D. Yi, and A. C. Brenner, "Mass gains of the Antarctic ice sheet exceed losses," *J. Glaciology*, vol. 61, no. 230, pp. 1019–1036, 2015.
[58] G. S. Hamilton and V. B. Spikes, "Assessing the performance of a satellite altimeter digital elevation model for Antarctica using precise kinematic GPS profiling," *Global Planetary Change*, vol. 42, nos. 1–4, pp. 17–30, 2003.
[59] ICESat Science Investigator-Led Processing System (I-SIPS). (Dec. 2014). *Attributes for ICESat Laser Operations Periods*. [Online]. Available: https://nsidc.org/sites/nsidc.org/files/files/glas_laser_ops_attrib.pdf
[60] W. Abdalati *et al.*, "The ICESat-2 laser altimetry mission," *Proc. IEEE*, vol. 98, no. 5, pp.735–751, May 2010.
[61] C. E. Webb, H. J. Zwally, and W. Abdalati, "The Ice, Cloud, and land Elevation Satellite (ICESat) summary mission timeline and performance relative to pre-launch mission success criteria," NASA Tech. Rep. NASA/TM-2013-217512, Dec. 2012.
[62] T. Urban, N. Pie, D. Felikson, and B. E. Schutz, "Impacts on Greenland and Antarctica ice sheet mass balance from estimation of ICESat-1/GLAS inter-campaign elevation biases over the oceans," in *Proc. EOS Trans. AGU, Fall Meeting Suppl.*, 2013.

Adrian A. Borsa is currently an Assistant Professor with the Institute of Geophysics and Planetary Physics, Scripps Institution of Oceanography, San Diego, CA, USA. His work aims to describe how the shape of Earth's surface is changing at timescales of seconds to decades, and to link observed change to geophysical processes associated with phenomena ranging from earthquakes to climate change. He is also actively involved in the calibration and validation of elevation measurements from several generations of satellite altimeters, and has made the remote salar de Uyuni, Bolivia, his field home for the past decade in support of this work. His research interests include the collection and analysis of geodetic data from many sources, including permanent and mobile GPS sensors, airborne lidar, and satellite altimeters.

Helen Amanda Fricker is currently a Professor with the Institute of Geophysics and Planetary Physics, Scripps Institution of Oceanography, University of California at San Diego (UCSD), San Diego, CA, USA. She uses a combination of satellite radar and laser altimetry and other remote-sensing data to understand ice sheet processes. She is widely recognized for her discovery of active subglacial lakes, and she has shown that these lakes form dynamic hydrologic systems, where one lake can drain into another in a short period of time. She is also known for her innovative research into Antarctic ice shelf mass budget processes such as iceberg calving and basal melting and freezing. She is also with the ICESat-2 Science Definition Team and the NASA Sea Level Change Team. Her research interests include ice sheets in Antarctica and Greenland and their role in the climate system.

Dr. Fricker is a member of the ICESat Science Team. She was a recipient of the Martha Muse Prize for Science and Policy in Antarctica from the Scientific Committee on Antarctic Research in 2010.

Kelly M. Brunt received the B.S. degree in geology from Syracuse University, Syracuse, NY, USA, in 1993, the M.S. degree in geology from the University of Montana, Missoula, MT, USA, in 1997, and the Ph.D. degree in geophysics from the University of Chicago, Chicago, IL, USA, in 2008, focusing on modeling ice-shelf flow and the connection between ice shelves, ice streams, and the ocean.

She was a Post-Doctoral Scholar with Scripps Institution of Oceanography, San Diego, CA, USA, where she was involved in the calibration and validation of Ice, Cloud, and land Elevation Satellite (ICESat) laser altimetry data. She is currently an Associate Research Scientist with the Earth Science Interdisciplinary Center (ESSIC), University of Maryland at College Park, College Park, MD, USA. She is also with the NASA Goddard Space Flight Center, Greenbelt, MD, USA, where she joined the Cryospheric Sciences Laboratory in 2010. She is involved in the planning for the postlaunch calibration and validation of ICESat-2 elevation data, and was involved with the MABEL high-altitude airborne laser altimeter designed as a simulator for ICESat-2.